symmetry

MDPI

Article

Dark Matter as a Result of Field Oscillations in the Modified Theory of Induced Gravity

Farkhat Zaripov

N. Lobachevsky Institute of Mathematics and Mechanics, Kazan Federal University, Kazan 420008, Russia; farhat.zaripov@kpfu.ru; Tel.: +7-903-344-6130

Received: 9 November 2019; Accepted: 16 December 2019; Published: 24 December 2019

Abstract: The paper studies the modified theory of induced gravity (MTIG). The solutions of the MTIG equations contain two branches (stages): Einstein (ES) and "restructuring" (RS). Previously, solutions were found that the values of such parameters as the "Hubble parameter", gravitational and cosmological "constants" at the RS stage, fluctuate near monotonously developing mean values. This article gives MTIG equations with arbitrary potential. Solutions of the equations of geodesic curves are investigated for the case of centrally symmetric space and quadratic potential at the RS stage. The oscillatory nature of the solutions leads to the appearance of a gravitational potential containing a spectrum of minima, as well as to antigravity, which is expressed by acceleration directed from the center. Such solutions lead to the distribution of the potential of the gravitational field creating an additional mass effect at large distances and are well suited for modeling the effect of dark matter in galaxies. The solutions of the equation of geodesic lines are obtained and analyzed. We found that the transition from flat asymptotics to oscillatory asymptotics at large distances from the center with a combination of the presence of antigravity zones leads to a rich variety of shapes and dynamics of geodesic curves and to the formation of complex structures.

Keywords: dark matter; symmetry; dark energy; cosmological constant; dark matter in galaxies

1. Introduction

This work is a continuation of the author's previous studies, which consider the modified theory of induced gravity (MTIG). The relevance of the work is due to the following problems.

1. In the opinion of most researchers, the presence of dark matter in and around galaxies is a well-established fact (see review [1]). The bulk of cosmological data in the commonly adopted model of the expanding Universe suggests the dominance of dark mass over the baryonic matter: the DM mass fraction is about a quarter of the total mass/energy, including dark energy, and the baryonic fraction is merely around 4–5%, which in turn is by an order of magnitude higher than the total mass of luminous matter concentrated in galaxies. Thus, both DM and most of the baryonic matter remains undiscovered by direct observations.

2. There is a problem of "accuracy of gravitational constant measurement" G. Despite the many experiments [2–4] to refine its value, the gravitational constant has not been determined even to the fourth decimal place. This fact suggests the possible variations of the parameter G depending on the coordinates of space-time.

3. Two methods are used to measure the Hubble constant. The first method is based on measuring the brightness of standard candles, the second method based on the analysis of CMB radiation. The first method shows a "local" rate of expansion in near our galaxy, and the second one provides information on the initial stage of evolution, 380,000 years after the Big Bang.The first method gives a value of $H_{local} = 73.48 \pm 1.66$ km·s^{-1} Mpc^{-1}, and the second—$H_{CMB} = 67.0 \pm 1.2$ km·s^{-1} Mpc^{-1}. These two

independent measurements give a discrepancy of approximately 9% This situation of inconsistency is called Hubble tension (see [5,6]). The measurement accuracy of H_{local} is about 4.5%.

In works [7,8], we presented a model in which, due to the oscillatory regime in the solutions of equations, the Hubble parameter also oscillates relative to the average value. In the article [8], we proposed, as a discussion, that for the later evolutionary time, the oscillation amplitudes of the Hubble constant should increase compared to previous times. From a numerical comparison with our various [8] models, it follows that this paradox is better explained by the so-called "stochastic models" (Purusha Universe in [7].

In this article we will show that a similar mechanism holds for solutions in a centrally symmetric space. The influence of anharmonic vibrations on the metric increases with increasing distance from the center, more precisely, from the point ($r = r_s$), where the deviation of the square of the scalar field (Z) from its vacuum value ($Z = 1$) is given as the boundary condition ($\Delta Z \simeq 10^{-6}$). This point is chosen close to the center and is located at a distance of the order of the gravitational radius (but a little further) of the central mass. For mass $M \approx 4 \cdot 10^6 M_\odot$ the deviation from the Schwarzschild-de Sitter solution becomes significant at distances greater than 0.07 kpc and leads to additional gravitational acceleration of the order of $10^{-10} \div 10^{-9}$ m/s^2.

We have shown that the quadratic potential of the scalar field and the inclusion of deviations of the metric from the Schwarzschild–De-Sitter metric up to the second order are essential factors for the realization of oscillatory solutions. This fact can be compared with studies of nonlinear stability in the anti-de Sitter (AdS) space. Despite the fact that the space-time AdS is linearly stable, unstable behavior occurs when quadratic perturbations are taken into account, which also lead to the emergence of new stable structures. The paper [9–11] states: "some initial data with a small amplitude remain small for a much longer (possibly for all) time, although other initial low-amplitude data ϵ collapse, after multiple reflections from the AdS boundary, to form black holes on time scales of the order of $1/\epsilon^2$". Similar conclusions were obtained for Einstein's vacuum equations in the anti-de Sitter space [12], where time-periodic solutions (geons) were postulated.

In order to try to solve the above problems and compare them with observations of DE and DM, a phenomenological model of the modified theory of induced gravity (MTIG) was proposed, which is described in our works [7,8,13–15]. In a simplified version of the theory, we made an attempt to introduce a certain macroscopic parameter of the theory Y, which generates both gravitational (G_{eff}) and cosmological (Λ_{eff}) "constants" [7]:

$$G_{eff} = G_{eff}(Y,\ U_{eff}), \qquad \Lambda_{eff} = 3U_{eff}, \tag{1}$$

where $U_{eff} = U_{eff}(Y)$—effective potential of the theory (note: the definition of U_{eff} in this article differs from its definition in articles [7,8]); G_{eff} some function of Y depending on the type of potential $U_{eff}(Y)$.

In our works [7], we compare the Newtonian gravitational constant (k_n) with the effective "gravitational constant".

$$\frac{8\pi k_n \hbar}{c^3} \equiv 6.5653 \cdot 10^{-65}\text{cm}^2 = G_{eff}(C_m), \tag{2}$$

where C_m is the value of the function $Y = Y(t_m)$ corresponding to the age of the Universe t_m; $\hbar$—Planck's constant, c—speed of light. The value of the cosmological constant (in length dimensions) is assumed to be equal $\Lambda_m \simeq 1.271 \cdot 10^{-56}/\text{cm}^2$, which approximately corresponds to observational data.

Attempts to find the value of C_m and its agreement with the values of all parameters of the theory (see [14]) did not lead to success because the number of parameters is too large. Not only for this reason, but because of the desire to maintain the scale invariance of the theory, we moved on to the model where we are trying to operate with dimensionless parameters, where possible. Therefore, from the function Y, which has the dimension of the square of the length (a priori, it was assumed that all quantities in action are determined through the dimension of the length), we switched to the

dimensionless function $Z = Y/C_m$. Given the certainty of the gravitational constant of not more than the fourth decimal place (described above as problem 2), the deviation condition is $|\Delta Z| \leq 10^{-4}$.

The concept of "induced gravity", first introduced by A.A. Sakharov in 1967, in the work [16] meant that gravity is not "fundamental" in the sense of elementary particle physics, but follows from quantum field theory (see [17–19]) .

In connection with an expanded understanding of the concept of "induced gravity", we want to mention the works of E. Verlinde [20,21], in which he attributes the attraction of two macroscopic bodies to an increase in total entropy with a decrease in the distance between the bodies. In other words, the system simply goes into a more probable macrostate.

In the context of our theory, the term "induced gravity" means that in the initial action the Einstein part $R/(2\kappa)$ is not introduced, since such a term arises due to the fixing of the function Y at the solutions of the equations.

The original version of the theory, the macroscopic parameter $Y \equiv (X, X) = X^A X^B \eta_{AB}$ represents a scalar product in D dimensional flat space-time Π with metric η_{AB}, with arbitrary signature; functions $X^A = X^A(\sigma^\mu)$, where $A, B = 1, 2, \ldots, D, \quad \mu, \nu = 0, 1, \ldots, n-1$, maps n dimensional Riemannian manifold M described by the metric $g_{\mu\nu}$, into space—time Π ([13]. The image of this mapping is an n-dimensional surface in space-time Π. Then, by analogy with string theory, we would get the theory of n branes, which has the property of conformal invariance for certain values of the parameter $\xi = \xi_0$. However, due to the mathematical difficulties associated with resolving the differential equations of coupling, this program is still far from being implemented. For further calculations we set $n = 4$.

Earlier [22], we obtained the following self-consistent equations:

$$G_{\alpha\beta} = \frac{1}{2\xi Y}[-\frac{n-2}{2}B + U]g_{\alpha\beta} + \frac{1}{Y}[\nabla_\alpha \nabla_\beta - g_{\alpha\beta}\Box]Y - \frac{w}{2\xi Y}T_{(e)\alpha\beta}, \tag{3}$$

where $G_{\alpha\beta}$—the Einstein tensor; $T_{(e)\alpha\beta}$ the EMT of matter fields (for example, perfect fluid); the consequence of these equations is the law of conservation of energy, which has the form:

$$-\frac{n-2}{2}\nabla_\beta B + \nabla_\beta Y \cdot (\xi R + \frac{dU}{dY}) - w\nabla_\alpha T^\alpha_{(e)\beta} = 0. \tag{4}$$

Initially, the theory was based on the desire to generalize string theory:

$$S_0 = \frac{1}{w}\int \left\{-\frac{\varepsilon}{2}(\nabla_\nu X, \nabla^\nu X) + \xi R(X, X) + U + L_m(X, S)\right\}\sqrt{-g}\hat{d}^n\sigma. \tag{5}$$

where w, ξ, ε there are constant; here fixing the Levi-Civita connection ∇ of the metric g; $(\nabla_\nu X, \nabla^\nu X) = \nabla_\nu X^A \nabla_\mu X^B g^{\nu\mu}\eta_{AB}$. For simplicity, in this paper $U(X^A) = U(Y(X^A))$. $L_m(X, S)$—characterizes all possible interactions X^A with other fields of matter. S_0 is conformal invariant for $\xi = \xi_0 \equiv -\frac{n-2}{8(n-1)}$, $\varepsilon = 1$, $U(Y) = \Lambda_X Y^2$.

In our previous works, the Equations (3) and (4) obtained from action (5) were considered under the following additional "embedding" conditions:

$$B_0 g_{\mu\nu} = (\nabla_\mu X, \nabla_\nu X) \quad \mu, \nu = \overline{0, n-1}. \tag{6}$$

To ensure the self-consistency of the equations, it was supposed to introduce unknown functions S^A, which affect the equations for $g_{\nu\mu}, Y$ only through EMT. This approach is not consistent and mathematically correct in order to say that Equation (3) (or (12) of the cited article [7]) are obtained from action (5) for $\varepsilon = 1$. We can assume that equations (3) are given phenomenologically, or they can be obtained from action (5) at $\varepsilon = 0$ and overriding the potential U on $\tilde{U}(Y) = U(Y) - \frac{n-2}{2}B$. In the latter case, from a mathematical point of view, everything is justified. We use action (5) for the case $\varepsilon = 1$ to indicate the further prospects of the theory. For example, we continue the study of this model for the case $\varepsilon = 1$, by introducing the Lagrange parameters, with the condition for constraints (6) to be

fulfilled. Thus, in this article, equations for individual fields X^A and constraints (6) are not considered at all.

In order to take into account the effect of vacuum polarization energy into gravity, we highlighted from EMT matter a part related to this energy, which satisfies the equation of state: $\varepsilon_{vac} + p_v = 0$, where ε_{vac} and p_v are interpreted as the energy density and vacuum polarization pressure. Therefore, in the equations (except for (6)) we made a substitution: $B_0 \Rightarrow B$,

$$B = \frac{n-2}{2} B_0 - w\varepsilon_{vac}. \tag{7}$$

Equations (3) can also be obtained by varying the action:

$$S_1 = \frac{1}{w} \int \left\{ \xi RY + \tilde{U}(Y) + L_m(Y, S) \right\} \sqrt{-g} \hat{d}^n \sigma, \tag{8}$$

by the metric g, where $\tilde{U}(Y) = U(Y) - \frac{n-2}{2} B$ is the new potential.

In this form, the action can be considered within the framework of the principle of P. A. Dirac, which reduces to the possible dependence of physical constants on each other, as well as on cosmological evolution. Modification of Einstein's equations by introducing an additional scalar field led to the creation of various versions of scalar-tensor theories of gravity. Among them, we note the Brans-Dicke theory [23], P. Jordan [24], J. Narlikar [25] and the conformally invariant scalar-tensor theories of gravity (see [26–29]). At the same time, the problem of breaking the conformal invariance of the theory arose, which was facilitated by the successful implementation of the principle of "spontaneous symmetry breaking" and the Higgs mechanism [30] for combining fundamental interactions. Based on this approach, studying the action (8) at the transition point $Y = const \leftrightarrow Y \neq const$ is of great interest. This transition is not trivial, but leads to the appearance of special instability. This can be seen from the equation (4), which for the case of this article has the form:

$$\nabla_\beta Y \cdot (\xi R + \frac{d\tilde{U}}{dY}) = 0, \quad B = const, \; L_m = 0. \tag{9}$$

The RS stage for the system is when we solve equation $\xi R = -d\tilde{U}/dY$. However, among the solutions of this equation, the solutions $Y = const$ may also be contained, depending on the parameters of the potential $\tilde{U}$. In this case, the RS and ES states are mixed.

We noticed that the system of Equation (3) can be rewritten so that for one of the equations we can take the Equation (9), which disappears when $Y = const$. Thus, we also explore solutions containing transitions from ES to RS and vice versa. As shown in previous papers, such solutions resemble phase transitions and contain elements of stochasticity [7].

The MTIG theory can be considered as some generalization of Einstein's theory of GR. Indeed, for the case $Y = const = C_m$, the MTIG equations are equivalent to the Einstein equations (GR) with a cosmological constant (ES stage). Small deviations of Y from the constant value of C_m can be investigated as deformations of the manifold M. It is clear that for small deviations, the experimental results of the theory of GR will be fulfilled with great accuracy in the theory of MTIG. It was surprising for us that in solutions for the RS stage in centrally-symmetric space, a noticeable difference from the GR theory occurs at large distances from the center $r > r_{cr}$.

Different models of dark energy and dark matter and their implications have recently been studied in the context of scalar-tensor theories [31–37] and also in the context of F(R) gravity [38]. The connection of dark energy with the thermodynamics of the Universe is studied in [37,39]. In works [40,41] the problems of dark energy oscillations are discussed, including their comparison with observational data [40], and it is also investigated which model of the various classes presented can create oscillations with the smallest amplitude [41].

Studies on the possibility of the phenomenon of antigravity were carried out in the works [42,43]. The article [43] it is noted: "... negative kinetic energy in antigravity presents no problems of principles but is an interesting topic for physical investigations of fundamental significance".

2. Centrally Symmetric Solutions

Let's consider the above Equations (3) with the potential $\tilde{U}(Y) = \Lambda_X Y^2 + f_w Y - B,\ B = const$, for a static centrally-symmetric space defined by the metric:

$$ds^2 = e^{\nu} dt^2 - e^{\lambda} dr^2 - r^2(d\theta^2 + sin^2(\theta) d\varphi^2), \tag{10}$$

where $\nu = \nu(r), \quad \lambda = \lambda(r), \quad T_{(e)\alpha\beta} = 0$. As follows from (3), the effective potential of the scalar field is $U_{eff} = (\Lambda_X Y + f_w - B/Y)/(2\xi)$.

From a comparison with the cosmological model, for the case $Y = C_m = const$, the cosmological constant is: $\Lambda_{eff} = U_{eff}(C_m)$. We fix the value of C_m equal to the modern cosmological value of Y and proceed to the dimensionless function $Z = Y/C_m$, after redefining the parameters: $f_n = f_w/(6\xi)$, $L_n = \Lambda_X C_m/(6\xi)$, $B_n = B/(6C_m\xi)$, we have $\Lambda_{eff}/3 = L_n + f_n - B_n$ and

$$U_{eff}(Z) = 3(L_n Z + f_n - B_n/Z). \tag{11}$$

For the case $Y = C_m$, the metric coincides with the Schwarzschild-de Sitter metric:

$$\nu_0(r) = -\lambda_0(r);\ e^{-\lambda_0(r)} = 1 - \frac{\Lambda_{eff}}{3} r^2 - \frac{r_g}{r},\ r_g = 2GM, \tag{12}$$

where Λ_{eff} at the *ES* stage is expressed, based on the cosmological solutions discussed in previous articles Refs. [7,8]. For the sake of brevity, we will not indicate the arguments of the functions, and the derivative with respect to r will be denoted by $(')$.

After the introduction of notation $Z = Z(r) = Y(r)/Y_0$, the Equations (3) in the metric (10) take the form:

$$G_0^0:\ -U_{eff}(Z) + e^{-\lambda}\left(\frac{\lambda' Z'}{2Z} + \frac{\lambda'}{r} - \frac{Z''}{Z} - \frac{2Z'}{Zr} - \frac{1}{r^2}\right) + \frac{1}{r^2} = 0; \tag{13}$$

$$G_1^1:\ -U_{eff}(Z) - \frac{e^{-\lambda}}{2Z} Z'\nu' - \frac{e^{-\lambda}}{r}\nu' - \frac{2e^{-\lambda}}{Zr} Z' - \frac{e^{-\lambda}}{r^2} + \frac{1}{r^2} = 0; \tag{14}$$

$$G_2^2 = G_3^3:\ -U_{eff}(Z) + e^{-lam}\left(-\frac{\nu'^2}{4} + \frac{\nu'\lambda'}{4} - \frac{\nu''}{2} - \frac{\nu' Z'}{2Z} + \frac{\lambda' Z'}{2Z} - \frac{\nu'}{2r} + \frac{\lambda'}{2r} - \frac{Z''}{Z} - \frac{Z'}{Zr}\right) = 0. \tag{15}$$

One of the equations that we will use to describe the *RS* stage is Equation (9). For *ES* stage the solutions Equations (4) are of the form (12).

For the case *RS* stage, by simplifying equations by means of algebraic actions, in [7] we obtained three independent equations for the functions $F(r),\ \lambda(r),\ Z(r)$. Instead of $\nu(r)$ we use the function $F(r) = \lambda(r) + \nu(r)$. Two of these are the first-order equations, one is the second-order equation:

$$F' = \frac{2r}{Z'r + 2Z}\left[Z'\left[\left(\left(U_{eff}(Z) - g(Z)\right) r - \frac{1}{r}\right) e^{\lambda} + \frac{Z'}{Z} - \frac{1}{r}\right] - 2Zg(Z)e^{\lambda}\right]; \tag{16}$$

$$\lambda' = \frac{2Z'r}{Z'r + 2Z}\left[\left(\left(U_{eff}(Z) - g(Z)\right) r - \frac{1}{r}\right) e^{\lambda} + \frac{Z'}{Z} + \frac{1}{r}\right] + \\ + \frac{2Z}{Z'r + 2Z}\left[e^{\lambda}\left(r\left(U_{eff}(Z) - 2g(Z)\right) - \frac{1}{r}\right) + \frac{1}{r}\right]; \tag{17}$$

$$Z'' = Z'\left[\frac{Z'}{Z} + e^{\lambda}\left[r\left(U_{eff}(Z) - g(Z)\right) - \frac{1}{r}\right] - \frac{1}{r}\right] - 2Ze^{\lambda}g(Z), \tag{18}$$

Here we introduced a new function $g \equiv g(Z) = f_n - 2B_n/Z$ and expressed the derivatives of the potentials through it: $dU_{eff}/dY = (U_{eff} - 3g)/Z$, $(d\tilde{U}/dY)/\xi = 4U_{eff} - 6g$.

Note that the Equations (16)–(18) (*RS* of the stage) also contain the solution $Z = Z_1 = const$, under the following condition on the parameters: $g(Z_1) = 0 \Longrightarrow f_n = 2B_n/Z_1$. At the points where this relation holds transitions from RS to ES are possible. However, we are not considering this issue yet. Based on the interest in this point of instability, and also because of the desire to reduce the number of parameters, we will use this relationship in various anzats in further calculations. In this article, we will use the following relation for constants: $f_n = 2B_n$. Then $g(Z_1) \div \triangle ZB_n \div B_n 10^{-6}$ is a small quantity.

Remark 1. *In the article [7] I missed the following typos related to the system of Equations (13)–(15): in formula (81) instead of the term f_n, write $3f_n$; in formula (83) instead of $e^{-\lambda}\lambda' Z'/Z$, write $e^{-\lambda}\lambda' Z'/(2Z)$; field potential is determined by a different sign than in this article (the parameters f_n, L_n, B_n are indicated with a different sign) . These typos are in no way connected with calculations and results.*

Numerical Solutions for Geodesic Lines

For a further numerical solution of obtained equations, we pass to the functions $F(r)$, $\alpha(r)$, $Z(r)$:

$$e^{\lambda(r)} = \frac{e^{\alpha(r)}}{T(r)};\ e^{\nu(r)} = e^{F(r)-\lambda(r)},\ T(r) \equiv 1 - \frac{\Lambda_{eff}}{3}r^2 - \frac{r_g}{r}, \tag{19}$$

where, $r_g = 2 \cdot GM$—gravitational radius, GM—central mass parameter. Direct calculations prove the following statement. *For a centrally symmetric metric given in the form (10),the equations of geodesic curves in the ecliptic plane ($\theta = \pi/2$) can be reduced to the (canonical) form:*

$$\frac{d^2r}{d\tau^2} = -\frac{1}{2}\frac{d}{dr}V_{\tau};\ v_{\tau}(r)^2 \equiv \left(\frac{dr}{d\tau}\right)^2 = E^2 - V_{\tau};\ \frac{d\varphi}{ds} = \frac{L_{\varphi}}{r^2}, \tag{20}$$

where, $E = const$, $L_{\varphi} = const$, $V_{\tau} \equiv \left(L_{\varphi}^2/r^2 + 1\right)e^{\nu(r)}$—the modified potential of the geodesic equation; instead of s the parameter τ is introduced: $ds/d\tau = e^{(\nu(r)+\lambda(r))/2}$.

The period of oscillation depends on the value of B_n. Its value for all calculations presented in this article is the same $B_n \approx 0.332$ kpc^{-2}, and was chosen because of a desire to receive a period of about 5.7∼6 kpc (at distances from r_{cr} to 50 kpc). An attempt at justification is given in [7].

Below are graphs of numerical solutions of the geodesic equation for parameter values indicated each time and invariable boundary conditions for solving Equations (16)–(18):

$$\alpha(s_0) = 0;\ F(s_0) = 0;\ Z(s_0) \equiv Z_1 = 1.000001238;\ Z'(s_0) = 0, \tag{21}$$

are given at the $s_0 \approx r_g \cdot (1 + 10^{-10})$ kpc.

The algorithm for numerical solution of the obtained equations is as follows. For the boundary condition (21), Equations (16)–(18) are solved numerically and the values of the field Z and metric functions are found: $G(r) = \{Z(r), Z'(r), F(r), \alpha(r)\}$. Then, initial conditions (22) are set for the complete system of Equations (16)–(18), (20), in which we pass from the variable r to the variable s (or τ) along the geodesic $r = r(s)$:

$$r(0) = r_2, Z(0) = Z_2, \dot{Z}(0) = p_2, F(0) = F_2, \alpha(0) = \alpha_2, v_r(0) = v_{20}, \phi(0) = 0, \tag{22}$$

where $\{Z_2, p_2, F_2, \alpha_2\} = G(r_2)$, dot means derivative with respect to s.

Figure 1 shows a graph of potential energy for mass $GM = 3.95 \cdot 10^6 GM_\odot$. In Figure 1a $r \in (0.09,\ 1)$; In Figure 1b $r \in (0.05,\ 55)$. The dashed line shows the potential for the Schwarzschild-de Sitter field, with the same values of the parameters.

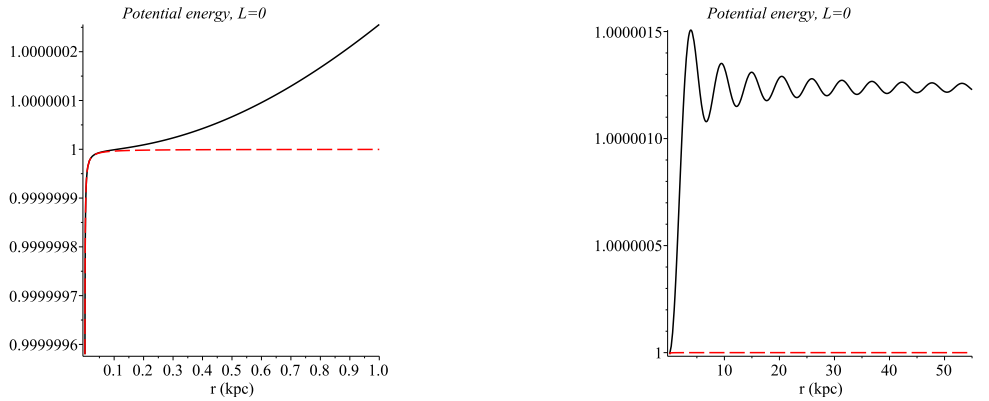

(**a**) (**b**)

Figure 1. Potential energy for mass $GM = 3.95 \cdot 10^6 GM_\odot$, $L_\phi = 0$; (**a**) $r \in (0.09,\ 1)$; (**b**) $r \in (0.05,\ 55)$.

In Figure 2 is a comparison of acceleration (solid line) with acceleration in the Schwarzschild metric (dashed line) (Figure 2a) and the transition to oscillations (Figure 2 b) for mass $GM = 3.95 \cdot 10^6 GM_\odot$. Acceleration (test body) with a positive sign corresponds to the movement from the center, and acceleration with a negative sign—to the center. Thus, zones of gravity and antigravity arise, which leads to an unusual distribution of the types of geodesic curves. The types of geodesic curves and the distribution of velocities (test bodies) are determined by the presence of many extrema of the potential of the gravitational field and their location in relation to each other and to the center. For speeds much less than the speed of light, the parameter "s" can be considered as a parameter of time.

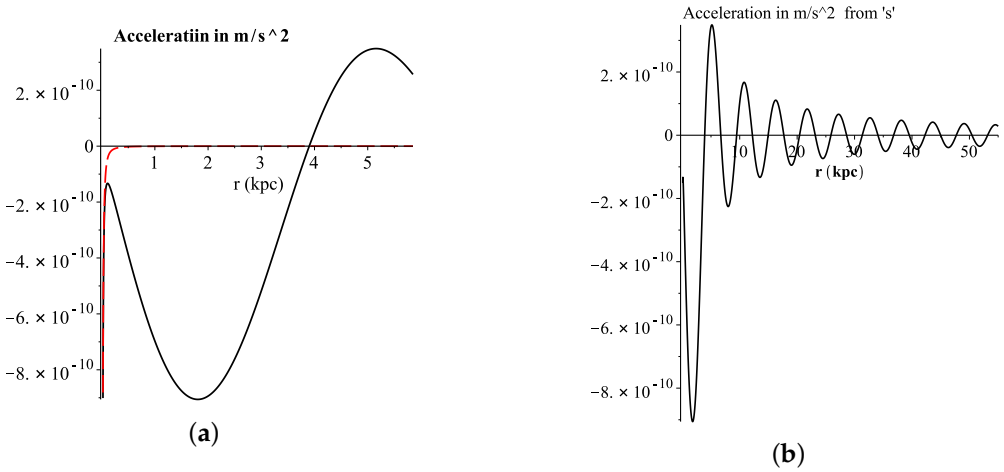

(**a**) (**b**)

Figure 2. Radial acceleration, with zero angular momentum, $GM = 3.95 \cdot 10^6 GM_\odot$; figure (**a**) for $r \in (0.025,\ 6.8)$ shows a comparison with the Schwarzschild solution (dashed line) and the transition to oscillations, figure (**b**) for $r \in (0.1,\ 55)$.

Approximate orbital velocities v_L (obtained from the equality of gravitational and centripetal forces) depending on distances are shown in Figure 3. These pictures are similar to the rotation curves of galaxies obtained from observational data. This is easily explained—acceleration from the center in the local zone can be combined with a fictitious mass located further from this zone (dark matter). In the first gravitational zone near the center, the motion along the geodesics differs little from motion in the Schwarzschild field. For (considered in this article) mass $GM = 10^{10} GM_\odot$

this zone can be conditionally limited by the radius $r_{cr} \approx 0.9$ kpc. This is the distance at which the acceleration difference in the MTIG theory from the acceleration calculated in the Schwarzschild metric is approximately equal to the acceleration itself. For the mass $GM \approx 4 \cdot 10^6 GM_\odot$ this radius is $r_{cr} \approx 0.1$ kpc (Figure 2a).

The dips in the orbital velocities in the figures of Figure 3b–d, correspond to antigravity zones where the velocity vector deviates from the tangent (for more details see in [7]). In these figures, we see that the number of such zones increases with distance, depending on the mass of the central body. For masses of the order of $10^8 GM_\odot$ or more, the widths of neighboring zones of gravity and antigravity are compared at distances greater than 50 kpc. For mass $3.95 \cdot 10^6 GM_\odot$ (Figure 3a , we see a quick transition to zones of the same width (but with different directions of acceleration relative to the center).

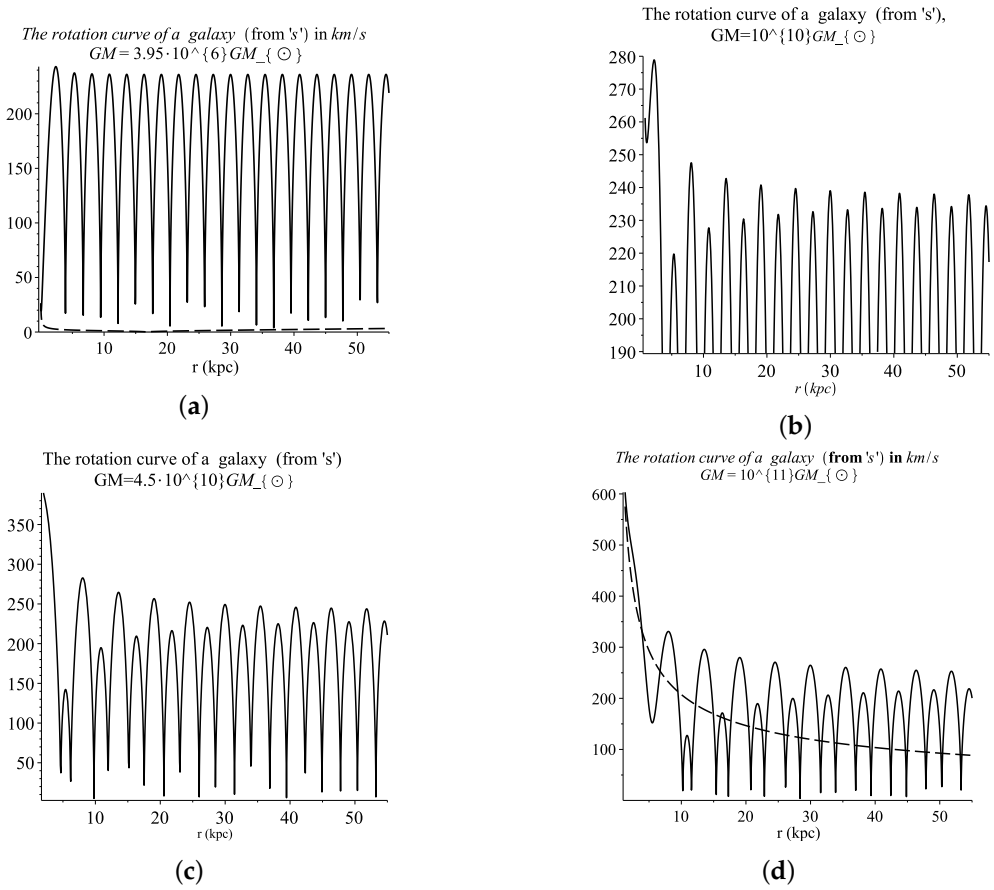

Figure 3. Galaxy rotation curve (v_L in km/s, for different central masses: (**a**) $GM = 3.95 \cdot 10^6 GM_\odot$; (**b**) $GM = 10^{10} GM_\odot$; (**c**) $GM = 4.5 \cdot 10^{10} GM_\odot$; (**d**) $GM = 10^{11} GM_\odot$. Dashed Lines—Keplerian speeds.

There are radii for which gravitational acceleration vanishes even in the absence of angular momentum ($L_\phi = 0$, see Figure 2) and initial velocity. Let R^i_{GA}, $i = 1, 2 \ldots$ and R^i_{AG} denote the radii for which the acceleration equals zero and changes sign from positive to negative and vice versa, respectively (see Figure 2a). The points and R^i_{AG} correspond to the minimum potential, as computer studies show, the circles $r = R^i_{AG}$, $\forall \phi$ are stable geodesics, and the circles $r = R^i_{GA}$, $\forall \phi$ are unstable.

As follows from Figure 2a, for the mass $3.95 \cdot 10^6 GM_\odot$, immediately after the point $r = r_{cr}$, there follows the gravity well G_w with additional acceleration to the center, and then a hump with acceleration from the center, with a maximum value compared to other antigravity extrema. Therefore, the instability point $r = R^1_{GA} \approx 3.901$ kpc separates internal orbits (around the center) with energies less than a certain value of E_{1a}, from external ones that are affected by acceleration from the center

and their trajectories are located (along the radius) further from the radius R^1_{GA}. In simple terms, the potential configuration in the vicinity of R^1_{GA} does not let some test bodies (with $E < E_{1a}$) move from the center, and the antigravity zone immediately after the point R^1_{GA} also does not allow bodies with energies below a certain value E_{1b} to move from the outer region to the center.

Figure 4 shows some geodesic curves internal relative to the radius R^1_{GA}. In Figure 4a shows a part of the curve over a period of 750 million years, with a small angular momentum $L = 0.00002$ kpc that intersects the zone G_w, approaching the center to distances of 0.016 kpc and moves most of the time near the circle $r = R^1_{GA}$. Near the center, the speed reaches 300 km/s and drops to zero near $r = R^1_{GA}$. Note that the orbit parameters for distances $r < r_{cr}$ from the point of view of Kepler's theory (also Schwarzschild's theory) would be classified as hyperbolic.However, at distances $r \geq r_{cr}$, due to the influence of additional acceleration in the G_w zone, the orbit becomes finite. Figure 4b,c show examples of stable geodesics corresponding to the zone G_w, the envelopes of the circles of which can come close to the circle $r = R^1_{GA}$ (Figure 4b).

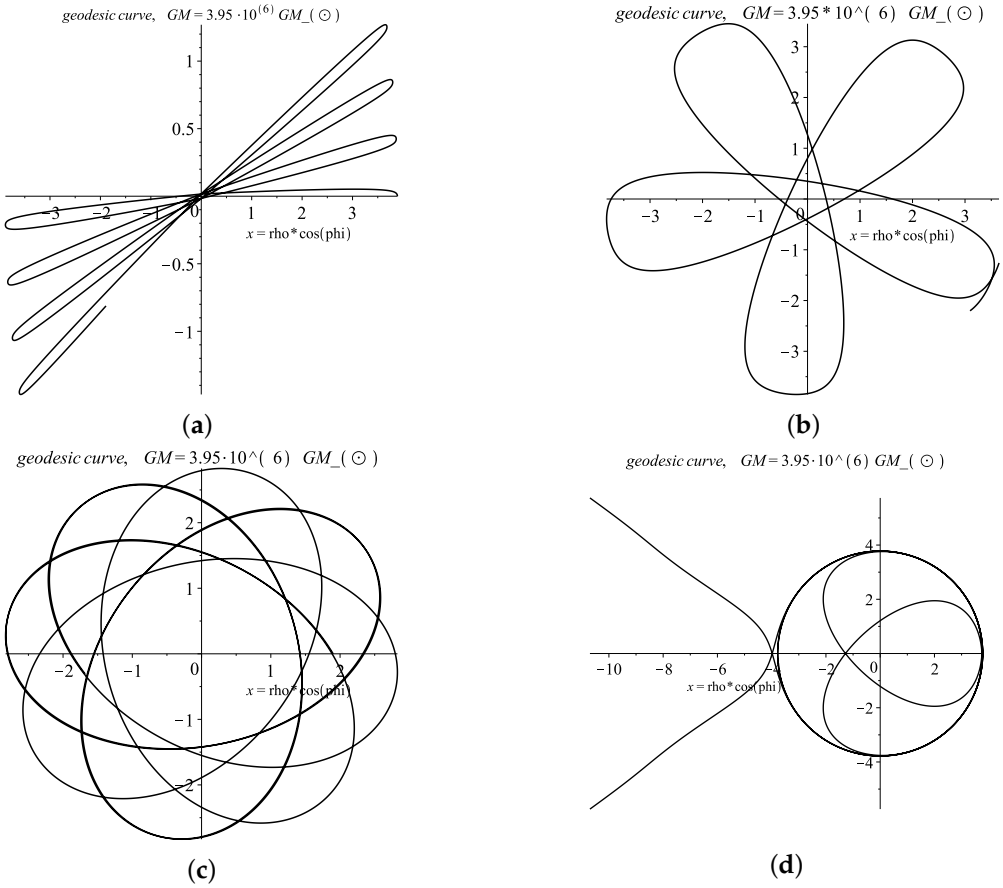

Figure 4. Geodesic curves, for initial conditions: (**a**) $r_2 \approx 3.89$ kpc, $v_{20} = 0$ km/s, $L_\phi \approx 2 \cdot 10^{-5}$ kpc; (**b**) $r_2 \approx 0.7$ kpc, $v_{20} = 304.05$ km/s, $L_\phi \approx 4.203 \cdot 10^{-4}$ kpc; (**c**) $r_2 \approx 1.9$ kpc, $v_{20} = -130$ km/s, $L_\phi = 0.001457675$ kpc; (**d**) $r_2 \approx 3.778358$ kpc, $v_{20} = 0$ km/s, $L_\phi \approx 0.001103125149$ kpc.

The exotic geodesic curve in Figure 4d shows a test body with a nonzero angular momentum and high radial velocity, moving from a distant region toward the center. After braking in the antigravity zone R^1_{GA}, receiving additional acceleration in the zone G_w, the body enters an almost circular unstable orbit $r \approx R^1_{GA}$, performs several revolutions and flies back from the center. The part of the curve for the period 1.2 billion years is given. This orbit was obtained by fitting parameters during a computer experiment. We specifically looked for examples of curves that are impossible in the Schwarzschild field in order to further try to find the corresponding observational confirmations in astronomy—inexplicable points of view of the standard theory of gravity. Another example that is

impossible from the point of view of the Schwarzschild model is shown in Figure 5a,b. Here, a test body moving from outside the galaxy toward the center at a speed of more than 200 km/s is repelled from the anti-gravity zone R^1_{GA} and flies out of bounds. The radial velocity depending on the radius for this geodesic is shown in Figure 5b.

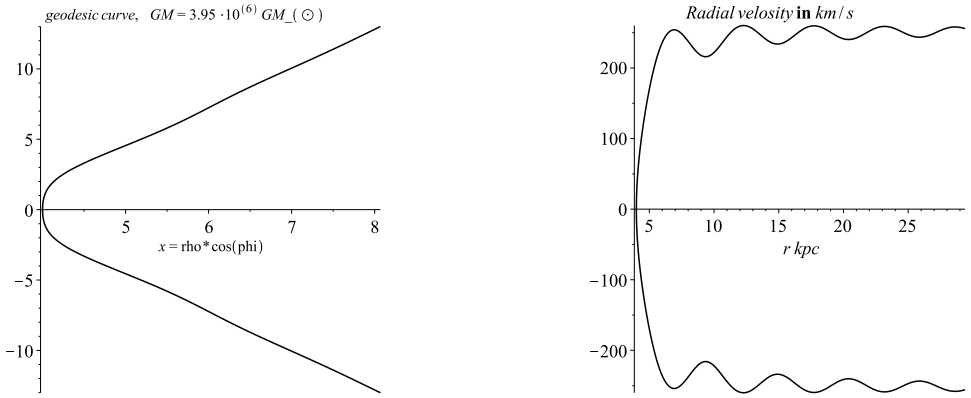

(**a**) (**b**)

Figure 5. (**a**) geodesic curve for initial values: $r_2 \approx 4$ kpc, $v_{20} = 0$ km/s, $L_\phi = 0.0026685$ kpc; (**b**) radial velocity versus radius.

For geodesics with zero or small angular momentum, oscillatory movements occur along the radius at the boundary of the transition from the antigravity zone to the gravitational zone ($r = R^i_{AG}$). Parts of geodesic curves are shown in the Figure 6. Here, a small value of the angular momentum is added only for the purpose of obtaining a solvable pattern in a rectangular coordinate system on the plane of motion. The Figure 6 shows parts of the graphs of geodesic curves for mass—$GM = 3.95 \cdot 10^6 GM_\odot$, angular momentum—$L_\phi \approx 6.6712819 \cdot 10^{-12}$ kpc, the initial speed is $v_{20} = 0$ km/s and for various initial values: (a) $r_2 = 5$ kpc—for the zone to the right of R^1_{AG}; (b) $r_2 = 10.5$ kpc—for the zone to the right of R^2_{AG}. Both graphs are given for 600 million years. A physical mechanism appears that accelerates matter (for example, gas, dust) towards each other and increases the temperature of the gas. In the above examples, this mechanism accelerates test bodies to speeds of 155 km/s and may be responsible for the star formation process. For this, it is necessary to take into account dissipative processes in gas flows and solve hydrodynamic equations, which we do not do. We can only make the assumption that the radial vibrational motion of gas flows and their interaction with flows having high circular velocities leads to the appearance of stable structures.

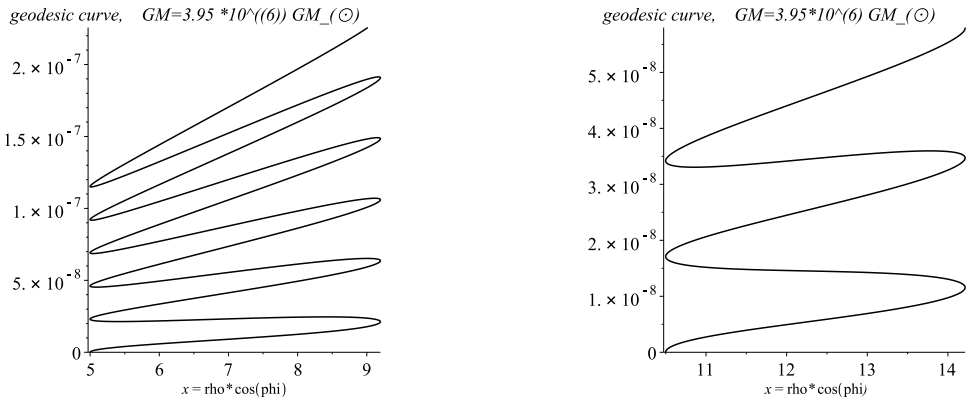

(**a**) (**b**)

Figure 6. Geodesic curves, for initial conditions: (**a**) $r_2 \approx 5$ kpc, $v_{20} = 0$ km/s, $L_\phi = 6.6712819 \cdot 10^{-12}$ kpc; (**b**) $r_2 \approx 10.5$ kpc, $v_{20} = 0$ km/s, $L_\phi = 6.671281904 \cdot 10^{-12}$ kpc.

Thus, in this model, we can assume a significant star formation outside the radius $R^1_{AG} \geq 4$ kpc from the center of the Galaxy. This assumption correlates with the conclusion based on astronomical observational data and given in [44]. Based on the lack of Cepheids in the inner part of the Galaxy, the authors of the work claim that there was no significant star formation in the radius of 2.5 kpc around the center of the galaxy for hundreds of millions of years.

With an increase in the angular momentum (angular velocity), the shape and dynamics of the geodesic curves are formed as a result of the orbital and oscillatory motion along the radius. There are a family of stable circular (or almost circular) orbits in the gravitational zones $R^i_{AG} < r < R^{i+1}_{GA}$, for the corresponding initial conditions: $r = r_2, v_2 = 0$ and the parameter L_ϕ. To obtain such curves, it is enough to use the graphs of Figure 3 and determine the corresponding rotation moment $L_{\phi 0} = r_2 v_L/c$, where v_L is circular rotation velocity corresponding to the radius r_2. As a comparison: for a distance of $r_2 = 8$ kpc, approximately equal to the radius of the Sun's rotation around the center of the galaxy, for a mass of $3.95 \cdot 10^6 GM_\odot$ the value is $v_L \approx 236$ kpc/s and for the mass $10^{10} GM_\odot$ the value is $v_L \approx 246$ kpc/s. The approximate rotation periods, respectively 203 and 210 million years. Thus, the rotational velocities are comparable, despite the huge difference in the value of the central masses. Without giving the circles themselves, in Figure 7 we give the geodesic trajectories for cases of deviation from the circles due to the addition of the initial radial velocity $v_2 = -15$ kpc/s, over a period of 1 billion years.

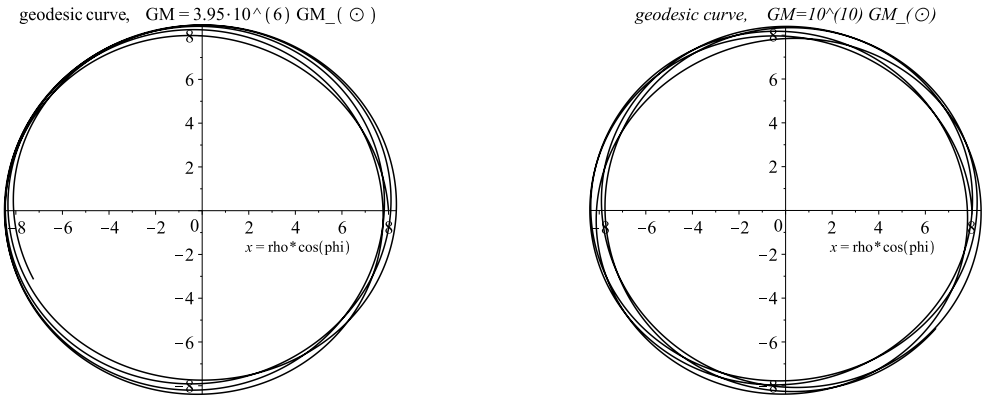

(**a**) (**b**)

Figure 7. Geodesic curves , for initial conditions: (**a**) $GM = 3.95 \cdot 10^6 GM_\odot$, $r_2 = 8$ kpc, $v_{20} = -15$ km/s, $L_\phi = 0.00547$ kpc; (**b**) $GM = 10^{10} GM_\odot$, $r_2 = 8$ kpc, $v_{20} = -15$ km/s, $L_\phi = 0.006584$ kpc.

In case of partial violation of the correspondence of the orbit parameters to the values for circular orbits, the geodesic curves may partially go into neighboring antigravity zones. If this zone is on the left ($r < R^i_{AG}$) and the total energy of the curve is less than the potential energy at the maximum of the anti-gravity zone, acceleration from the center returns the curve back to a stable region. Thus, the orbits located closer (in their orbital parameters) to the point R^i_{AG} are more stable than the orbits near the point R^i_{GA}. This resistance to changing parameters (for example, v_2 and v_L) depends on the ratio of the heights of neighboring potential highs and lows. For example, we give the trajectories of closed geodesics (Figure 8), for the initial conditions corresponding to the second half of the antigravity zone and with less energy—so as not to slip through the following gravitational zones of attraction (right). Figure 8 shows the trajectory and radial velocity for a geodesic differing from the previous case only in angular momentum: $GM = 10^{10} GM_\odot$, $r_2 = 8$ kpc, $v_{20} = -15$ km/s, $L_\phi \approx 0.00480693$ kpc—this angular momentum corresponds to the circular velocity $v_L = 180$ km/s at a distance of 8 kpc.

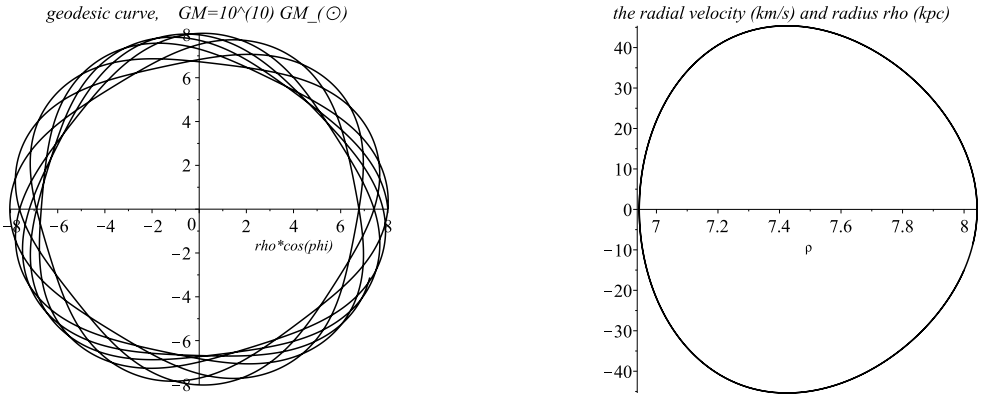

(**a**) (**b**)

Figure 8. (**a**) geodesic curve and (**b**) radial velocity depending on radius for initial values: $GM = 10^{10} GM_{\odot}$, $r_2 = 8$ kpc, $v_{20} = -15$ km/s, $L_{\phi} \approx 0.00480693$ kpc.

Figure 8 shows the trajectory (over a period of 1600 million years) and radial velocity for a geodesic differing from the previous case only in angular momentum: $GM = 10^{10} GM_{\odot}$, $r_2 = 8$ kpc, $v_{20} = -15$ km/s, $L_{\phi} \approx 0.00480693$ kpc—this angular momentum corresponds to the circular speed $v_L = 180$ kpc/s at a distance of 8 kpc. Thus, with decreasing angular momentum, the step width along the radius increases (in Figure 8 this width is about 1.25 kpc) and the radial velocity. The type of geodesic line in Figures 8a and 4a is the most common. There are rare limiting cases of such trajectories leading to exotic closed forms, some of which are shown at the end of the article (see Figure 9).

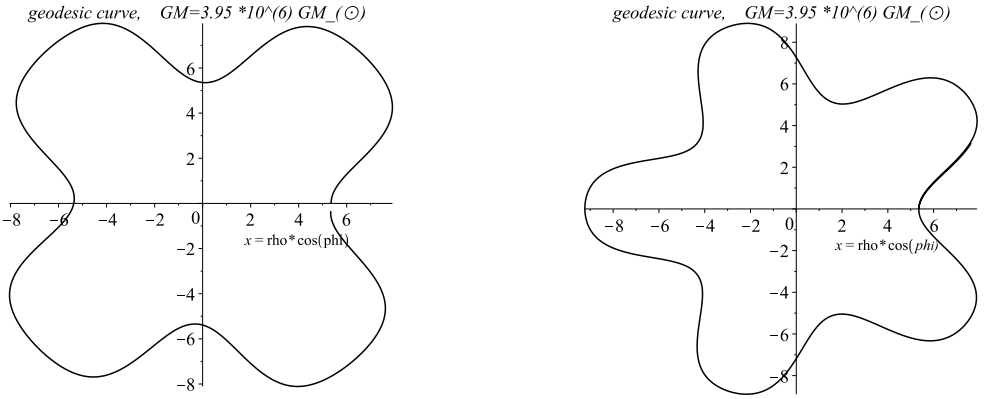

(**a**) (**b**)

Figure 9. Geodesic curves, $GM = 3.95 \cdot 10^6 GM_{\odot}$ for initial conditions: (**a**) $r_2 = 5.34998$ kpc, $v_{20} = 0$, $L_{\phi} \approx 0.001935333888$ kpc; (**b**) $r_2 = 5.355$ kpc, $v_{20} == 0$, $L_{\phi} \approx 0.001927466767693$ kpc.

3. Conclusions and Discussion

The solutions of the MTIG equations for the centrally symmetric metric, in addition to the Schwarzschild solution for $Z = 1$, contain a branch that goes over to the oscillatory mode at large distances. For distances $r << r_{cr}$, the observed characteristics of the gravitational field coincide with the characteristics of the Schwarzschild solution. For example, for the mass $GM = 10^{10} GM_{\odot}$, the deviation of acceleration from acceleration in the Schwarzschild field at a distance of 10^{-4} kpc is 10^{-13} km/s, and then decreases linearly with decreasing r, amounting to an order of 10^{-16} km/s at a distance of 10^{-7} kpc. At large distances, where (presumably) the influence of the galaxy is compared by the influence of other galaxies and the Schwarzschild field can be completely neglected, the vibrational regime continues to operate and the acceleration amplitude remains at the level of $A_{as} \simeq 10^{-10}$ km/s, regardless of the central mass. This fact leads to reflection on the use of the theory in question to describe the large-scale structure of the Universe.

In works [45–47], a team of authors report that they have discovered a galaxy in which dark matter is almost completely absent. On the other hand, there are a lot of data on other galaxies, indicating that they almost entirely consist of dark matter [5,48].

Recall that the mass parameter in the Schwarzschild solution appears as a certain constant of integration of the Einstein differential equations in the void. As you know, the same solutions can be obtained if we introduce matter proportional to $GM\delta(r)$ on the right side of the Einstein equations, where $\delta(r)$ is the Dirac delta function, which, from the point of view of mathematics, replaces the boundary condition at the point $r = 0$. By analogy, with the approach by which the mass parameter is introduced and with the assignment of $\Delta Z = Z - 1$ as the boundary condition, we can hypothesize the existence of some hidden parameter responsible for the asymptotic behavior of the gravitational field at large distances.

Unfortunately, we do not yet have analytical solutions to the MTIG equations and cannot find all the integration constants. Instead, we can consider ΔZ as a parameter responsible for gravity in the far asymptotic, along with mass. In the general case, the deviations of the characteristics of the gravitational field from the same characteristics for the case of the Schwarzschild solution depend on the boundary condition on the field Z. A boundary condition is imposed near the event horizon, in order to simplify computer calculations related to the singularity (this is not important, it is important that it is near the center). Smaller $|\Delta Z|$—leads to smaller deviations from the Schwarzschild solution and to smaller values of the oscillation amplitude.

It is shown that in the vicinity of the galaxy, at least three types of zones can be distinguished. For $r_g > r < r_{cr}$, this is the Schwarzschild zone, where the behavior of geodesics, with an accuracy of the order of $10^{-9} \div 10^{-10}$, does not differ from the Schwarzschild solutions, although it is possible to design experiments to detect them. Further, the zones of antigravity and gravity are periodically repeated with increasing $r > r_{cr}$. We have obtained many solutions for orbits that are impossible in the theory of Newton and Einstein. Comparison of such solutions with unexplained astronomical observations is the task of subsequent research. For example, we can recall the effect of the "pioneers" (see works [49,50]), which is associated with the problem of additional gravitational acceleration at the far reaches of the Solar system, at the free flight of space probes "Pioneer -1" and "Pioneer -2" .

We found that the transition from flat asymptotics to oscillatory asymptotics at large distances from the center with a combination of the presence of antigravity zones leads to a rich variety of shapes and dynamics of geodesic curves and to the formation of complex structures. This emphasizes the value of further research in the studied direction of research and the importance of searching for experimental data on measuring the gravitational potential far from the center without reference to the value of the central mass.

Funding: The research was funded by the subsidy allocated to Kazan Federal University for the state assignment in the sphere of scientific activities, project N. 1.13556.2019/13.1.

Conflicts of Interest: The author declares no conflict of interest.

Abbreviations

The following abbreviations are used in this manuscript:

GR	General relativity
MTIG	Modified Theory of Induced Gravity

References

1. Zasov, A.V. ; Saburova, A.S.; Khoperskov, A.V.; Khoperskov, S.A. Dark matter in galaxies. *Phys. Usp.* **2017**, *60*, 3–40. doi:10.3367/UFNr.2016.03.037751. [CrossRef]
2. Speake, C.; Quinn, T. The search for Newton's constant. *Phys. Today* **2014**, *67*, 27–33. [CrossRef]
3. Rosi, G.; Sorrentino, F.; Cacciapuoti, L.; Prevedelli, M.; Tino, G.M. Precision measurement of the Newtonian gravitational constant using cold atoms. *Nature* **2014**, *510*, 518–521. [CrossRef] [PubMed]

4. Li, Q.; Chao, X.; Liu, J.-P.; Wu, J.-F.; Yang, S.-Q.; Shao, C.-G.; Quan, L.-D.; Tan, W.-H.; Tu, L.-C.; Liu, Q.; et al. Measurements of the gravitational constant using two independent method. *Nature* **2018**, *560*, 582–588. [CrossRef] [PubMed]
5. Riess, A.G.; Macri, L.M.; Hoffmann, S.L.; Scolnic, D.; Casertano, S.; Filippenko, A.V.; Tucker, B.E.; Reid, M.J.; Jones, D.O.; Silverman, J.M.; et al. Determination of the Local Value of the Hubble Constant. *Astrophys. J.* **2016**. [CrossRef]
6. Riess, A.G.; Casertano, S.; Yuan, W.; Macri, L.; Anderson, J.; Mackenty, J.W.; Bowers, J.B.; Clubb, K.I.; Filippenko, A.V.; Jones, D.O.; et al. New Parallaxes of Galactic Cepheids from Spatially Scanning the Hubble Space Telescope: Implications for the Hubble Constant. *arXiv* **2018**, arXiv:1801.01120. doi:10.3847/1538-4357/aaadb7.
7. Zaripov, F. The Ambiguity in the Definition and Behavior of the Gravitational and Cosmological 'Coupling Constants' in the Theory of Induced Gravity. *Symmetry* **2019**, *11*, 81. [CrossRef]
8. Zaripov, F. Oscillating Cosmological Solutions in the Modified Theory of Induced Gravity. *Adv. Astron.* **2019**, *2019*, 15. [CrossRef]
9. Bizon, P.; Rostworowski, A. On weakly turbulent instability of anti-de Sitter space. *Phys. Rev. Lett.* **2011**, *107*, 031102. [CrossRef]
10. Maliborski, M.; Rostworowski, A. Lecture notes on turbulent instability of anti-de Sitter spacetime. *Int. J. Mod. Phys. A* **2013**, *28*, 1340020. [CrossRef]
11. Craps, B.; Evninb, O.; Vanhoof, J. Ultraviolet asymptotics and singular dynamics of AdS perturbations. *JHEP* **2015**, *1510*. [CrossRef]
12. Dias, O.J.C.; Horowitz, G.T.; Santos, J.E. Gravitational Turbulent Instability of Anti-de Sitter Space. *Class. Quant. Grav.* **2012**, *29*, 194002. [CrossRef]
13. Zaripov, F.S. A conformally invariant generalization of string theory to higher-dimensional objects. Hierarchy of coupling constants. *Gravit. Cosmol.* **2007**, *13*, 273–281.
14. Zaripov, F. Modified equations in the theory of induced gravity. *Astr. Space Sci.* **2014**, *352*, 289–305. 10509-014-1909-8. [CrossRef]
15. Zaripov, F.S. Phenomenological Model of Multiphase Cosmological Scenario in Theory of Induced Gravity. *Russ. Phys. J.* **2017**, *59*, 1834–1841. [CrossRef]
16. Sakharov, A.D. Vacuum Quantum Fluctuations in Curved Space and the Theory of Gravitation. *Sov. Phys. Dokl.* **1968**, *12*, 1040; Reprinted in *Gen. Rel. Grav.* **2000**, *32*, 365–367. [CrossRef]
17. Visser, M. Sakharov's Induced Gravity: A Modern Perspective. *Mod. Phys. Lett.* **2002**, *17*, 977. [CrossRef]
18. Andrianov, A.A.; Andrianov, V.A.; Giacconi, P.; Soldati, R. Induced gravity and universe creation on the domain wall in five-dimensional space-time. *Theor. Math. Phys.* **2006**, *148*, 880. [CrossRef]
19. Linnemann, N.S.; Visser, M.R. Hints towards the Emergent Nature of Gravity. *arXiv* **2018**, arXiv:1711.10503v2.
20. Verlinde, E. On the origin of gravity and the laws of Newton. *J. High Energy Phys.* **2011**, *2011*, 1. [CrossRef]
21. Verlinde, E. Emergent gravity and the dark universe. *SciPost Phys.* **2017**. [CrossRef]
22. Zaripov, F.S. Generalized equations of induced gravity. The evolution of coupling constants. *Vestnik TGGPU* **2010**, *4*, 23–28. (In Russian)
23. Brans, C.; Dicke, R.H. Mach's principle and relativistic theory of gravitation. *Phys. Rev.* **1961**, *124*, 925. [CrossRef]
24. Jordan, P. *Schwerkraft and Weltall*; Friedrich Vieweg und Sohn: Braunschweig, Germany, 1955.
25. Narlikar, J.V. Lepton creation and the Dirac relationship between fundamental constants. *Nature* **1974**, *247*, 99–100. [CrossRef]
26. Scholz, E. Weyl geometry in late 20th century physics. *arXiv* **2011**, arxiv:1111.3220v1.
27. Aviles, A.; Gruber, C.; Luongo, O.; Quevedo, H. Cosmography and constraints on the equation of state of the Universe in various parametrizations. *Phys. Rev. D* **2012**, *86*, 123516. [CrossRef]
28. Aalbers, J. Conformal Symmetry in Classical Gravity. 2013. Available online: http://dspace.library.uu.nl/handle/1874/280136 (accessed on 20 November 2018).
29. Carballo-Rubio, R. Longitudinal diffeomorphisms obstruct the protection of vacuum energy. *Phys. Rev. D* **2015**, *91*, 124071. [CrossRef]
30. Dengiz, S.; Tekin, B. Higgs Mechanism for New Massive Gravity and Weyl Invariant Extensions of Higher Derivative Theories. *Phys. Rev. D* **2011**, *84*, 024033. [CrossRef]

31. Nojiri, S.I.; Odintsov, S.D. Introduction to Modified Gravity and Gravitational Alternative for Dark Energy. *Int. J. Geom. Methods Mod. Phys.* **2007**, *4*, 115–145. [CrossRef]
32. Bamba, K.; Capozziello, S.; Nojiri, S.; Odintsov, S.D. Dark energy cosmology: the equivalent description via different theoretical models and cosmography tests. *Astrophys. Space Sci.* **2012**, *342*, 155–228. [CrossRef]
33. Moraes, P.H.R.S.; Sahoo, P.K. Wormholes in exponential f(R, T) gravity. *Eur. Phys. J.* **2019**, *79*. [CrossRef]
34. Nojiri, S.I.; Odintsov, S.D. Accelerating cosmology in modified gravity: From convenient F(R) or string-inspired theory to bimetric F(R) gravityInt. *J. Geom. Methods Mod. Phys.* **2014**, *11*, 1–24. [CrossRef]
35. De Rham, C.; Dvali, G.; Hofmann, S.; Khoury, J.; Pujolàs, O.; Redi, M.; Tolley, A.J. Cascading Gravity: Extending the Dvali-Gabadadze-Porrati Model to Higher Dimension. *Phys. Rev. Lett.* **2008**, *100*, 251603. [CrossRef] [PubMed]
36. Luongo, O.; Muccino, M. Speeding up the Universe using dust with pressure. *Phys. Rev. D* **2018**, *98*, 103520. [CrossRef]
37. Peter, K.; Dunsby, S.; Luongo, O.; Reverberi, L. Dark Energy and Dark Matter from an additional adiabatic fluid. *Phys. Rev. D* **2016**, *94*, 083525.
38. De Felice, A.; Tsujikawa, S. f(R) theories. *Liv. Rev. Relativ.* **2010**. [CrossRef]
39. Capozziello, S.; Luongo, O.; Pincak, R.; Ravanpak, A. Cosmic acceleration in non-flat f(T) cosmology. *arXiv* **2018**, arXiv:1804.03649.
40. Ringermacher, H.I.; Mead, L.R. Observation of Discrete Oscillations in a Model-Independent Plot of Cosmological Scale Factor versus Lookback Time and Scalar Field Model. *Astron. J.* **2015**, *149*, 137. [CrossRef]
41. Odintsov, S.D.; Oikonomou, V.K.; Sebastianie, L. Unification of constant-roll inflation and dark energy with logarithmic R2-corrected and exponential F(R) gravity. *Nucl. Phys.* **2017**, *923*, 608–632; doi.org/10.1016/j.nuclphysb.2017.08.018 [CrossRef]
42. Kamenshchik, A.Y.; Pozdeeva, E.O.; Starobinsky, A.A.; Tronconi, A.; Venturi, G.; Vernov, S.Y. Transformations between Jordan and Einstein frames: Bounces, antigravity, and crossing singularities. *Phys. Rev. D* **2016**, *94*, 063510. [CrossRef]
43. Bars, I.; James, A. Physical interpretation of antigravity. *Phys. Rev. D* **2016**, *93*, 044029. [CrossRef]
44. Matsunaga, N.; Feast, M.W.; Bono, G.; Kobayashi, N.; Inno, L.; Nagayama, T.; Nishiyama, S.; Matsuoka, Y.; Nagata, T. A lack of classical Cepheids in the inner part of the Galactic disc. *MNRAS* **2016**, *462*, 414–420. [CrossRef]
45. Van Dokkum, P.; Abraham, R.; Romanowsky, A.J.; Brodie, J.; Conroy, C.; Danieli, S.; Zhang, J. Extensive globular cluster systems associated with ultra diffuse galaxies in the Coma cluster. *Astrophys. J. Lett.* **2017**, *844*, L11. [CrossRef]
46. Van Dokkum, P.; Cohen, Y.; Danieli, S.; Kruijssen, J.M.D.; Romanowsky, A.J.; Merritt, A.; Abraham, R.; Brodie, J.; Conroy, C.; Lokhorst, D.; et al. A galaxy lacking dark matter. *Nature* **2018**, *555*, 629–632. [CrossRef] [PubMed]
47. Van Dokkum, P.; Cohen, Y.; Danieli, S.; Kruijssen, J.M.D.; Romanowsky, A.J.; Merritt, A.; Abraham, R.; Brodie, J.; Conroy, C.; Lokhorst, D.; et al. An Enigmatic Population of Luminous Globular Clusters in a Galaxy Lacking Dark Matter. *Astrophys. J. Lett.* **2018**, *856*, L30. [CrossRef]
48. Van Dokkum, P.; Abraham, R.; Brodie, J.; Conroy, C.; Danieli, S.; Merritt, A.; Mowla, L.; Romanowsky, A.; Zhang, J. A High Stellar Velocity Dispersion and 100 Globular Clusters for the Ultra Diffuse Galaxy Dragonfly 44. *Astrophys. J. Lett.* **2016**, *828*, L6. [CrossRef]
49. Anderson, J.D.; Laing, P.A.; Lau, E.L.; Nieto, M.M.; Turyshev, S.G. Search for a Standard Explanation of the Pioneer Anomaly. *Mod. Phys. Lett. A* **2002**, *17*, 875–885. [CrossRef]
50. Nieto, M.M.; Anderson, J.D. Using Early Data to Illuminate the Pioneer Anomaly. *Class. Quant. Grav.* **2005**, *22*, 5343–5354. [CrossRef]

© 2019 by the author. Licensee MDPI, Basel, Switzerland. This article is an open access article distributed under the terms and conditions of the Creative Commons Attribution (CC BY) license (http://creativecommons.org/licenses/by/4.0/).